Experimental study of directional detection of neutrons and gamma rays using an elpasolite scintillator array

A. Guckes [a,*], A. Barzilov [b], P. Guss [c]

[a] *Nevada National Security Site, North Las Vegas Operations, P.O. Box 98521, M/S NLV-068, Las Vegas, Nevada 89193-8521, USA, guckesal @nv.doe.gov, 1-702-295-0199*
[b] *University of Nevada Las Vegas, 4505 S. Maryland Parkway, Las Vegas, NV 89154, USA*
[c] *Nevada National Security Site, Remote Sensing Laboratory - Nellis, P.O. Box 98521, M/S RSL-09, Las Vegas, NV 89193-8521, USA*
[*] *Corresponding author*

Highlights

- Detection system based on elpasolite CLYC scintillators was studied for directional detection of neutrons and gamma rays.
- Experimental study of the scintillator responses was carried out using a three-cell array.
- Maximum likelihood estimation technique was used to localize a radiation source.
- Three-cell array is feasible to ascertain the direction to a neutron source and a gamma-ray source.

Abstract

A radiation detection system consisting of an array of three $Cs_2LiYCl_6:Ce^{3+}$ elpasolite cells was studied for simultaneous, directional neutron and gamma-ray measurements. Utilizing a neutron source and gamma-ray sources, measurements were carried out while rotating the three-cell array 360°. The measurement data was processed using a maximum likelihood estimation technique to determine the most probable angle pointing to the radioactive source. The detection system enables measuring gamma rays and neutrons simultaneously and estimating locations of radioactive sources within 23°.

Keywords: Elpasolite scintillator; CLYC; directional detector; neutron measurements; gamma spectroscopy.

1. Introduction

Radiation measurement systems are important to preventing nuclear weapons proliferation and supporting homeland security tasks such as detection, quantification and tracing of radioactive sources including nuclear materials [1-4]. Radiological and nuclear materials can be smuggled into countries through seaports and border crossings [5]. Radioactive sources have been stolen or lost exposing the public to elevated levels of radiation [6]. Radioactive isotopes can be discharged into the environment because of natural catastrophes or accidents at facilities such as the disaster at the Fukushima Daichi nuclear power plant [7-10]. In remote monitoring, photon and neutron measurements are utilized because charged particles such as electrons and alpha particles are attenuated by a thin shielding layer and have short ranges in air. Gamma and neutron detection are essential for nuclear waste management and environmental safety [11, 12], active material assay technologies [13-15], and dual-particle imaging techniques [16, 17]. It is imperative to continue to advance gamma and neutron detection capabilities to prevent and mitigate growing radiological and nuclear threats and support radiation measurement technologies for applications in different areas.

One such advancement in radiation detection is the ability to simultaneously detect neutrons and gamma rays using a single detector. Previously, two separate detection systems were employed: one system for the gamma spectroscopy, and another system for neutron counting. For example, a high purity germanium detector with cryocooling or a sodium iodide scintillator was used to measure a gamma spectrum, and a ^{3}He tube equipped with

a moderator was employed for neutron measurements [18]. The use of two different detectors with coupled electronics, power supplies, and software makes the gamma/neutron sensing system complex, bulky, and costly. Therefore, a dual mode (gamma rays and neutrons) detection system, preferably an ambient temperature design, is necessary especially for deployment in field conditions. Liquid and plastic scintillators enable detecting both photons and neutrons by a single sensor; however, their energy resolution is poor for the gamma spectroscopy [19-21].

The elpasolite scintillator $Cs_2LiYCl_6:Ce^{3+}$ (CLYC) allows gamma and neutron detection with no cryogenic cooling needed [22-24]. CLYC's density is 3.31 g/cm^3. The refractive index is 1.81 at 405 nm. CLYC is a bright scintillator; its outputs are 20,000 photons per one absorbed 1-MeV gamma ray and 70,000 photons per one absorbed thermal neutron. Gamma rays interact with the CLYC primarily by means of Compton scattering, photoelectric absorption, and pair production. The full width at half maximum (FWHM) energy resolution for 662 keV gamma rays is less than 5%. Thermal neutron detection is achieved via ^{6}Li(n,α)t reaction (the cross-section is 940 barns). The α-particle and ^{3}He ion share energy of 4.78 MeV, generating ionization tracks in CLYC. The trapping of free charges in Ce^{3+} scintillation centers leads to the de-excitation with production of a light pulse. In the energy spectrum, the associated peak is recorded at 3.0 MeV gamma-equivalent energy (GEE) with the FWHM energy resolution of 3%. It enables pulse height discrimination of neutron and photon events, except the 3-MeV electron equivalent (MeVee) peak width region. In addition to the detection of gamma rays and thermal neutrons, fast neutron spectroscopy with CLYC is feasible via (n,p) reaction on ^{35}Cl isotope leading to production of ^{35}S [25, 26]. The Q-value of this reaction is 0.615 MeV; the emitted proton's energy is the incident neutron energy plus the Q-value. The resultant peak appears at a GEE proportional to the incident neutron energy. This has been demonstrated for fast neutrons with an incident energy greater than 0.8 MeV up to 20 MeV. However, this reaction was not exploited in this study.

The CLYC scintillation emission includes three distinct decay components [27, 28]. Two components appear due to gamma ray interactions with the CLYC scintillator and include the core-to-valence luminescence (CVL) [29] and prompt Ce^{3+} emission. The CVL has 250 nm – 350 nm wavelength range and 2 ns decay time constant. The Ce^{3+} emission wavelength range is 350 nm – 450 nm, and the decay time constant is 50 ns. The third component that appears due to a neutron interaction within the CLYC is cerium self-trapped excitation (Ce-STE). It has 350 nm – 450 nm range and 1,000 ns decay time constant. The substantial difference in the decay times of the gamma-ray induced versus neutron-induced emission components of CLYC allows for an excellent pulse shape discrimination (PSD) between neutrons and gamma rays [30, 31]. To increase thermal neutron detection efficiency, the ^{6}Li-enriched CLYC crystals were grown. For example, the 95% ^{6}Li enriched CLYC (or CLYC6 material) enabled 2.3 times larger thermal neutron detection efficiency compared to ^{3}He gas of the same volume at 9.86 atmospheres [32].

Directional gamma and neutron detection systems that make it possible to locate positions of the sources are often needed [33-37]. Elpasolite detectors can be used for directional detection of photons and neutrons [38, 39]. Computational studies showed that a directional detection system consisting of an array of elpasolite detectors is feasible for simultaneous measurements of neutron and photon flux with the localization of radiation sources [40]. A detection system consisting of an array of three CLYC6 cells was developed and utilized in this study to experimentally ascertain the feasibility of such a system to address the directional sensing of gamma rays and neutrons simultaneously. Gamma spectroscopy, neutron/gamma PSD, and radiation source localization were performed. The experimental setup and test results are discussed herein.

2. Directional neutron and photon measurements

2.1 Experimental setup

An array of three cylindrical CLYC6 scintillator cells was developed. The array consisted of two 1-inch diameter by 1-inch height scintillators (denoted as CLYC #1 and CLYC #2) and one 1.5-inch diameter by 1.5-inch height CLYC scintillator (denoted as CLYC #3). The scheme of the three-cell array arranged as a symmetrical, tightly packed assembly is shown in Fig. 1. Elpasolite scintillator cells in this arrangement shadow each other

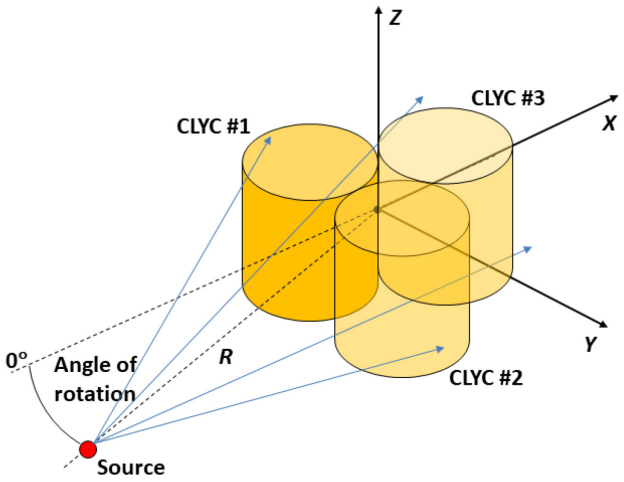

Figure 1. Scheme of the directional detection system.

partially blocking an incident photon or neutron at different angles. Therefore, incident gamma rays and neutrons generate different responses in the CLYC6 cells at different angles. This information enables deducing the angle pointing to the emitting source.

CLYC6 scintillators used in this study were procured from Radiation Monitoring Devices, Inc. To characterize each cell, neutron/gamma PSD and gamma spectroscopy measurements were carried out using a bialkali Hamamatsu R6231-100-01HA photomultiplier tube (PMT) matching the scintillation emission range of CLYC, high voltage (HV) base and a single-channel eMorpho digitizer (Bridgeport Instruments, LLC). The analog signals of the PMT anode were digitized. Then, the digital waveforms were analyzed yielding the following three parameters in a list mode: a waveform's start time, an integral under the waveform that is related to the energy of radiation absorbed in the CLYC cell, and 'partial' integral calculated only under the prompt portion of the signal based on the preset time window. These list-mode parameters were used for the neutron/gamma PSD analysis utilizing a radiation identification (RID) value calculated as a ratio of integrals under the tail portion and prompt portion of the waveform. Because neutron-induced waveforms exhibit longer tail parts than photon-induced waveforms, and similar rise times, the 'neutron' RID values are greater. It allows separating neutron events and photon events based on RIDs.

This study was performed at the nuclear engineering laboratory of University of Nevada Las Vegas. The laboratory houses a shielded vault containing radioactive sources: a moderated 2-Curie ^{239}PuBe source, 0.898-μCi ^{137}Cs and a 0.9314-μCi ^{60}Co gamma check sources. Photon only list-mode data were used to generate the gamma energy spectrum. The spectrum was calibrated using gamma test sources. The FWHM energy resolution of the 662 keV peak for ^{137}Cs and 1.17 MeV and 1.33 MeV peaks for ^{60}Co were determined employing a Gaussian fit.

2.2 Source localization

The source localization measurements were performed with an array of three CLYC scintillators each with its own PMT and HV base. A four-channel qMorpho MCA/digitizer (Bridgeport Instruments) was used to analyze signals of the three CLYC cells. Both digitizers were linked via USB to a PC running the Igor Pro user interface providing communication between the user and the detection system and processing capabilities to analyze the measured radiation data. All three detectors were mounted on to a rotating turntable that provided 360° rotation of the detectors in the *xy*-plane. For gamma measurements only, a source holder was used to move the source being detected along the *z*-axis (vertically). This was done to evaluate how varying the position of the source along the *z*-axis impacted the estimate of the source location in the *xy*-plane. These three-dimensional measurements of the gamma-ray sources are representative of how the detector system would respond to a source in the field that is not

in the plane of the detection system. The ^{239}PuBe source shown in Figure 8 was too heavy to move along the *z*-axis. Thus, the ^{239}PuBe source was not moved along the *z*-axis.

For each source placement scenario, the detector system was rotated 360° in the *xy*-plane in increments of 40°. Data gathered from each detector in the three-cell array at each angle was processed using a maximum likelihood estimation (MLE) procedure. The MLE methodology is a statistical analysis that provides means to estimate unknown parameters for a set of data [41]. In this study, it is the angle pointing to a radioactive source location that was estimated using MLE. The angular dependent data measured by each CLYC cell in the three-cell array was fitted with a sum of sine model. Both the data and the resultant fits for each measurement are shown in Figure 5, 7, and 9. The angle at which each fitted function has a maximum, ϕ_m , is the most probable source angle for the *m*-th detector, where *m* = 1, 2, or 3, assuming that each detector will observe the maximum number of counts when the greatest amount of each detector's surface area is exposed to the radiation emitted from the source. It is also the angle at which an individual detector is least shielded from the source by the other two detectors. It was also assumed that the observed source direction obtained from each detector in the array is normally distributed with the probability density function (PDF):

$$P(\phi_m \,|\theta, \sigma^2) = \frac{1}{\sqrt{2\pi}\sigma} \exp \frac{-(\phi_m - \theta)^2}{2\sigma^2} \tag{1}$$

where θ is the predicted source angle (unknown), and σ^2 is the variance of θ. Since all cells are independent, the PDF for the angle pointing to the source considering all three cells in the array is:

$$P(\{\phi_m\}_{m=1}^{3} \,|\theta, \sigma^2) = \prod_{m=1}^{3} P(\phi_m \,|\theta, \sigma^2) \tag{2}$$

The likelihood function of Eq. 2 is defined as:

$$Lf(\theta, \sigma^2) = ln[P(\{\phi_m\}_{m=1}^{3} \,|\theta, \sigma^2)] \tag{3}$$

The maximum likelihood estimate for the source angle is a θ value that maximizes the likelihood function:

$$\hat{\theta} = \arg\max_{\theta} Lf(\theta, \sigma^2) \tag{4}$$

The variance of $\hat{\theta}$ is defined as:

$$\hat{\sigma}^2 = \frac{1}{3} \sum_{m=1}^{3} (\phi_m - \hat{\theta})^2 \tag{5}$$

The standard deviation can be deduced from the variance. The angle from the detector system to the neutron or gamma-ray source being evaluated was known in this study. However, if this system would be deployed in the field to find a lost, stolen, or smuggled radioactive source or nuclear material, the exact position of the source will not be known prior to the measurements. By comparing the MLE evaluated angle to the actual angle representing the course location, it can be determined how well this detector system would find a radioactive source of unknown location in the field.

3. Results and discussion

3.1 Pulse shape discrimination

Experiments of pulse shape discrimination of neutrons and photons were performed exposing the CLYC6 cells to a beam emitted by a moderated ^{239}PuBe (α,n) source. Fig. 2a shows a PSD plot of RID versus energy, with the energy scale in keVee (electron equivalent) units calibrated using gamma sources. Neutron/photon separation is excellent on this plot. A figure of merit (FOM) was used to denote how well a CLYC6 detector can segregate neutrons from gamma rays via PSD. The PSD FOM of a detector was calculated as $FOM = T / (W_1 + W_2)$, where T is the distance between the centroids of the peaks of particle 1 (gamma rays) and particle 2 (thermal neutrons), W_1 is the FWHM of the peak of particle 1 and W_2 is the FWHM of the peak of particle 2 (see Fig. 2b). A FOM of 2.3 was achieved for CLYC6 cells in this study. Particles are considered adequately separated with a FOM ≥ 1.27 [42]. Thus, the detected neutrons and gamma rays were successfully separated. The PSD technique can be utilized to perform simultaneous detection of both thermal neutrons and gamma rays using the developed detector system.

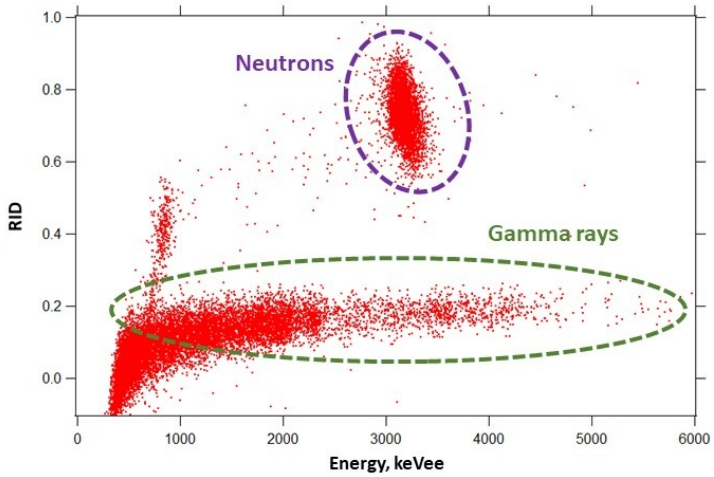

(a)

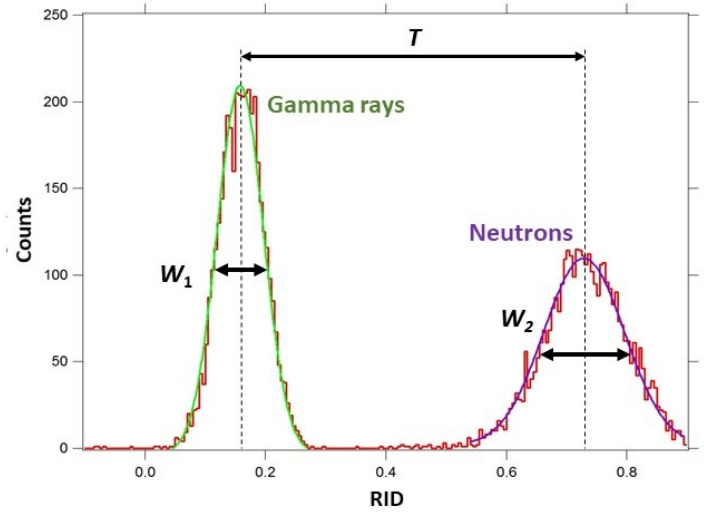

(b)

Figure 2. (a) Neutron/gamma PSD measurement for the CLYC cell using a moderated ^{239}PuBe source; **(b)** the neutron/gamma PSD FOM plot.

3.2 Gamma spectroscopy

The gamma-ray energy spectra of ^{137}Cs and ^{60}Co were recorded using photon data separated via PSD from neutron data. The spectra for a 1-in diameter by 1-in height CLYC cell are shown in Fig. 3a,b. A Gaussian fit of the ^{137}Cs peak at 662 keV (shown in blue) yields an energy resolution of 4.9% with approximately 1,496 counts in the peak area. The Gaussian fit of the characteristic gamma-ray energy peak of 1.17 MeV for ^{60}Co yields an energy resolution of 3.86% with approximately 816 counts. The Gaussian fit for the characteristic gamma-ray energy peak of 1.33 MeV ^{60}Co yields an energy resolution of 3.6% with approximately 812 counts. The measured resolution agrees with published data for CLYC elpasolites. Such energy resolution enables spectroscopic analysis of gamma emitters and their quantification.

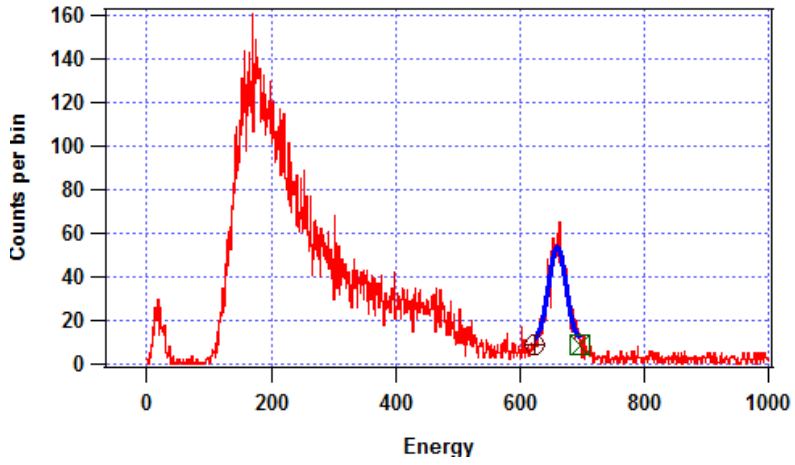

(a)

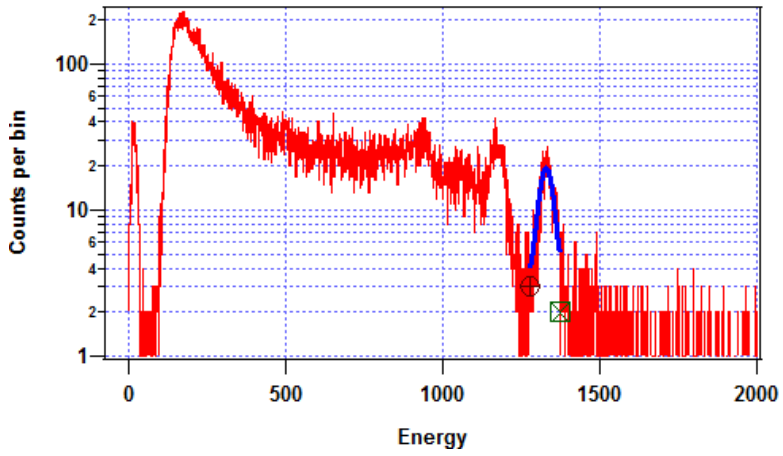

(b)

Figure 3. Gamma energy spectrum: **(a)** ^{137}Cs with Gaussian fit at the 662 keV peak and **(b)** ^{60}Co 1.33 MeV peak.

3.3 Source localization

Directional measurements were carried out using the three-cell detector system with the ^{137}Cs and ^{60}Co gamma-ray sources and the ^{239}PuBe neutron source in various configurations. The results of all configurations for the source localization measurements are summarized in Table 1.

It should be noted that CLYC cell #1 is centered with the 40° mark on the detector system turntable, CLYC #2 is centered with the 160° mark, and CLYC #3 is centered with the 280° mark. Thus, 40° will be subtracted from the direction for which the maximum counts occur for CLYC #1, 160° for CLYC #2, and 280° for CLYC #3 to obtain the inputs to the MLE algorithm. Since the CLYC cell #3 contained a larger CLYC scintillator (1.5-inch diameter by 1.5-inch height), all results for CLYC #3 were normalized to those of CLYC #1 and CLYC #2 so that the results would not be skewed.

The first configuration was with the ^{137}Cs source placed in plane (i.e., $z = 0$ cm) with the three CLYC scintillators and at the distance $R = 10$ cm from the center of the detector system as shown in Fig. 4. The source was placed at the 0°/360° mark on the detector system turntable. The results of directional measurements for this configuration are presented in Fig. 5a. The resulting MLE evaluated direction to the source was 5°.

The ^{137}Cs source was kept at the 0°/360° mark, but the distance from the center of the detector system and height were varied. Measurements were performed for the following three configurations: (1) $R = 20$ cm and $z = 0$ cm, (2) $R = 10$ cm and $z = +10$ cm, and (3) $R = 20$ cm and $z = +10$ cm. The results for these three configurations are presented in Fig. 5b,c,d, respectively. For $R = 20$ cm and $z = 0$ cm, the MLE source direction was 345° ± 2°. This estimate deviated from the actual source direction by 15°. For source position at $R = 10$ cm and $z = +10$ cm, the MLE source direction was 337° ± 16°. This deviated from the actual source direction by 23°. For $R = 20$ cm and $z = +10$ cm, the MLE evaluation of the source direction was 6° ± 26°. This result deviated from the actual direction by 6°.

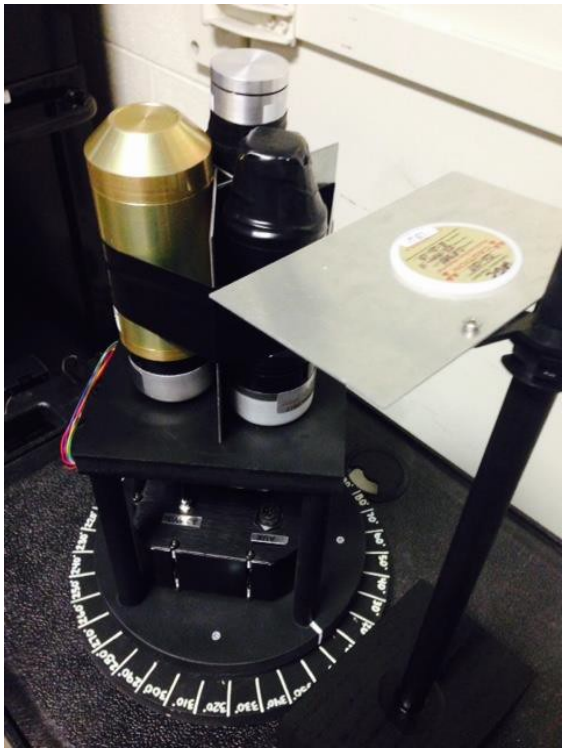

Figure 4. ^{137}Cs directional measurement.

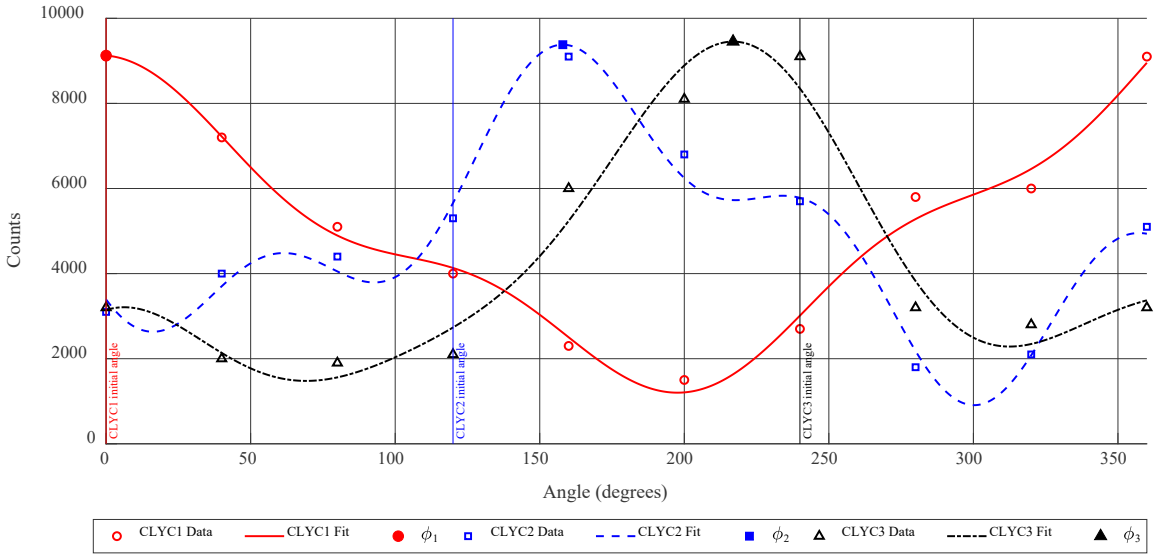
10000
8000
6000
4000
2000
0
Counts
0
50
100
150
200
250
300
350
Angle (degrees)
CLYC1 initial angle
CLYC2 initial angle
CLYC3 initial angle
CLYC1 Data
CLYC1 Fit
ϕ_1
CLYC2 Data
CLYC2 Fit
ϕ_2
CLYC3 Data
CLYC3 Fit
ϕ_3

(a)

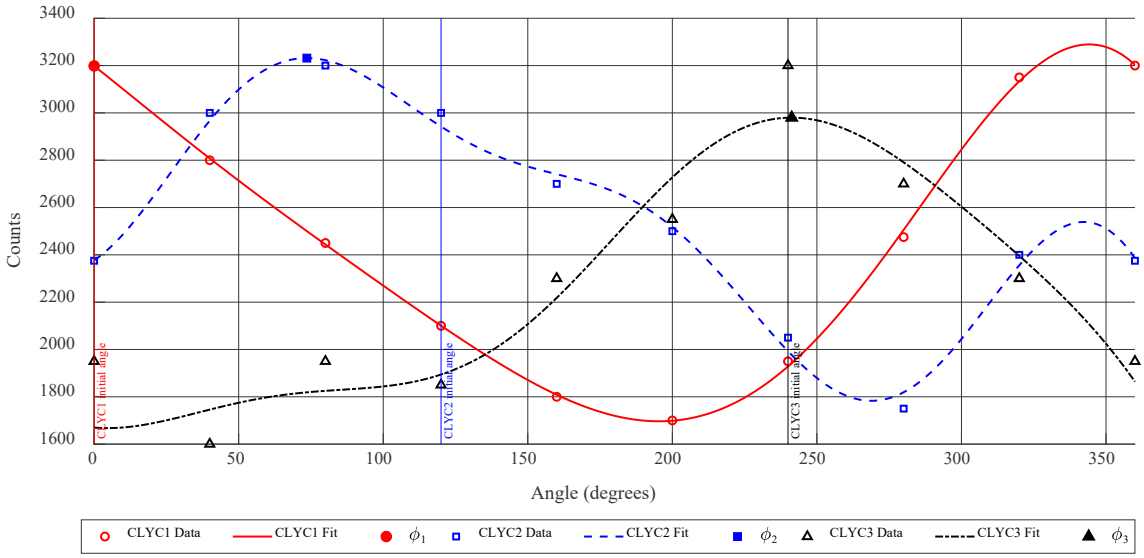
3400
3200
3000
2800
2600
2400
2200
2000
1800
1600
Counts
0
50
100
150
200
250
300
350
Angle (degrees)
CLYC1 initial angle
CLYC2 initial angle
CLYC3 initial angle
CLYC1 Data
CLYC1 Fit
ϕ_1
CLYC2 Data
CLYC2 Fit
ϕ_2
CLYC3 Data
CLYC3 Fit
ϕ_3

(b)

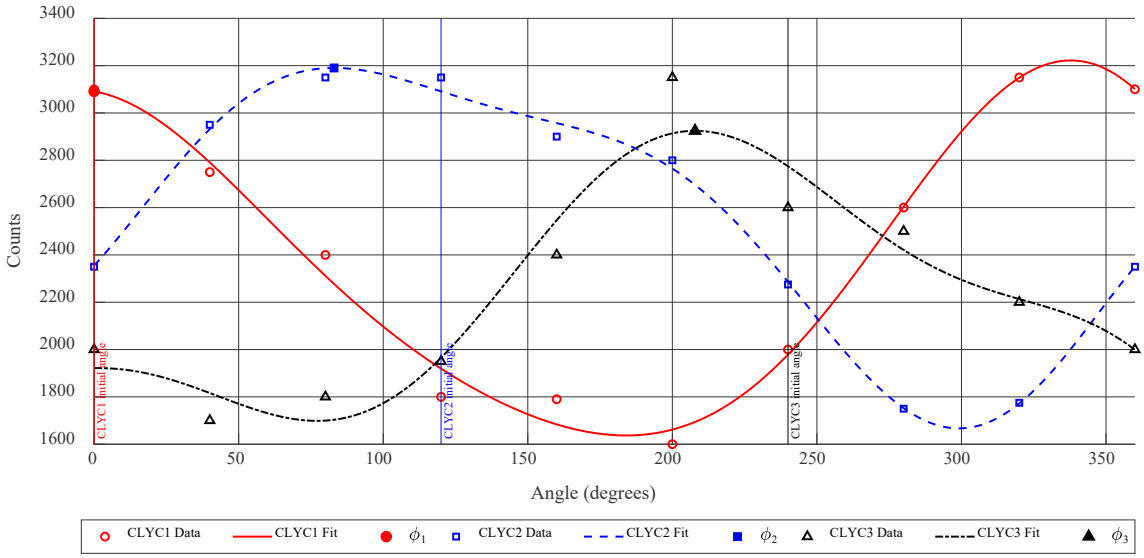

(c)

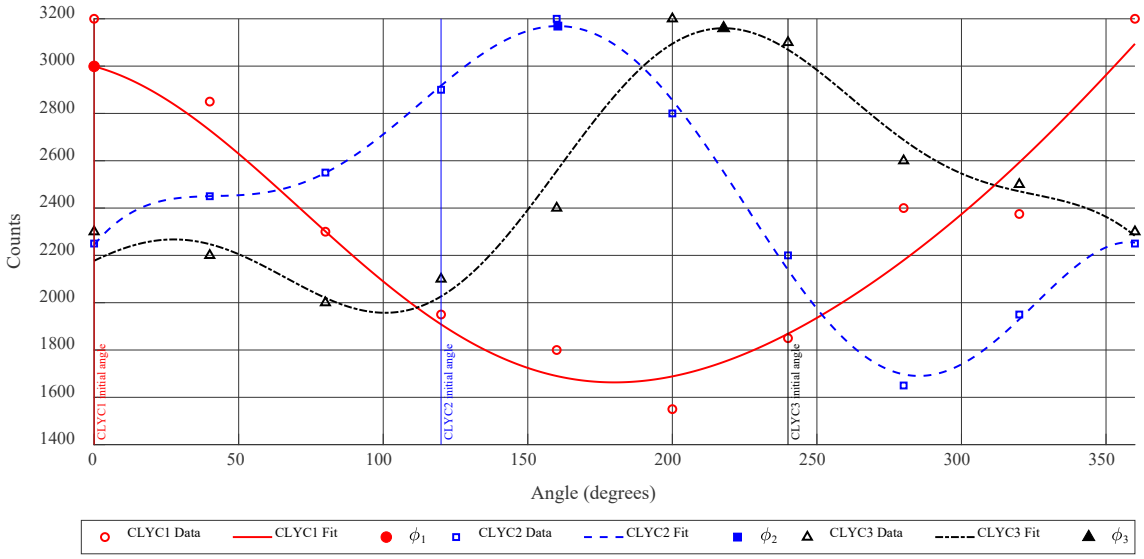

(d)

Figure 5. Directional measurement using a ^{137}Cs source placed at **(a)** R = 10 cm, z = 0 cm; **(b)** R = 20 cm, z = 0 cm; **(c)** R = 10 cm, z = +10 cm; **(d)** R = 20 cm, z = +10 cm.

A configuration consisting of both the ^{137}Cs and ^{60}Co gamma-ray sources was used as well. The ^{137}Cs source was placed at the 0°/360° mark on the turntable in plane with the CLYC scintillators (z = 0 cm) and at a distance of R = 10 cm from the center of the system. The ^{60}Co source was placed at the 240° mark of the turntable 20 cm below the plane of the detector system (z = -20 cm) and at R = 10 cm from the center of the directional detector. This setup is shown in Fig. 6. The results for the ^{137}Cs source directional measurements are presented in Fig. 7a. The results for the ^{60}Co source directional measurements are shown in Fig. 7b for the 1.17 MeV peak and Fig. 7c for the 1.33 MeV peak.

Figure 6. Two sources (^{137}Cs and ^{60}Co): directional measurement experimental setup.

For the ^{137}Cs source, the MLE source direction was 13° ± 8°. This estimate deviated from the actual source direction by 13°. For the ^{60}Co 1.17 MeV peak, the MLE source direction was 254° ± 6°. This deviated from the actual source direction by 14°. For the ^{60}Co 1.33 MeV peak, the MLE source direction was 250° ± 1°. This deviated from the actual source direction by 10°. The ^{60}Co source was also placed on top of the ^{137}Cs source to determine the feasibility of detecting two collocated gamma sources. The MLE estimates of the source direction for both sources agreed with the actual source direction of 0°/360°.

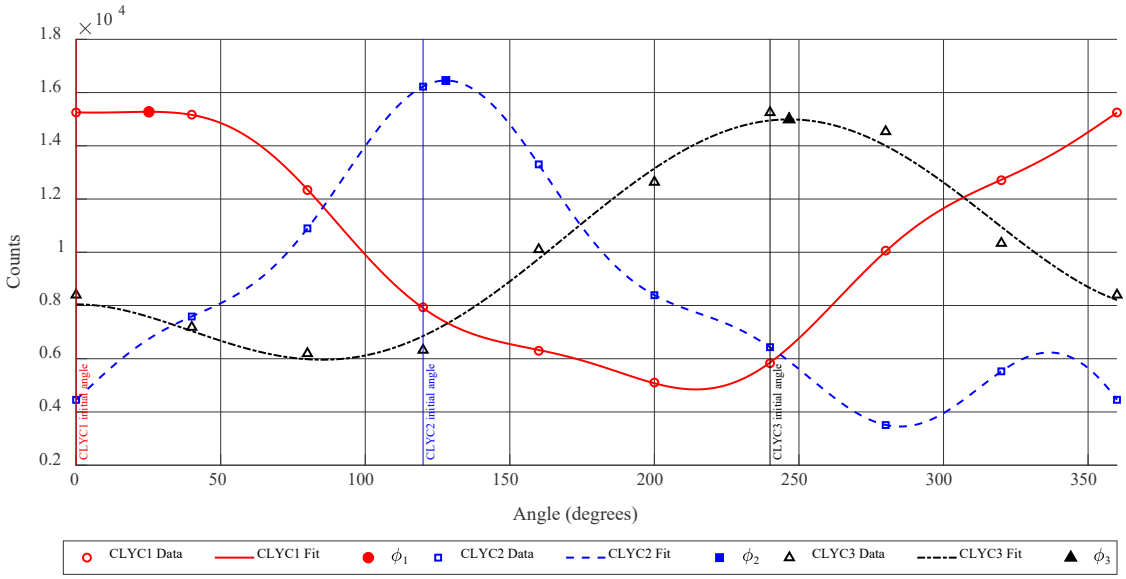
×10 4
1.8
1.6
1.4
1.2
1
0.8
0.6
0.4
0.2
Counts
CLYC1 initial angle
CLYC2 initial angle
CLYC3 initial angle
0
50
100
150
200
250
300
350
Angle (degrees)
CLYC1 Data
CLYC1 Fit
ϕ_1
CLYC2 Data
CLYC2 Fit
ϕ_2
CLYC3 Data
CLYC3 Fit
ϕ_3

(a)

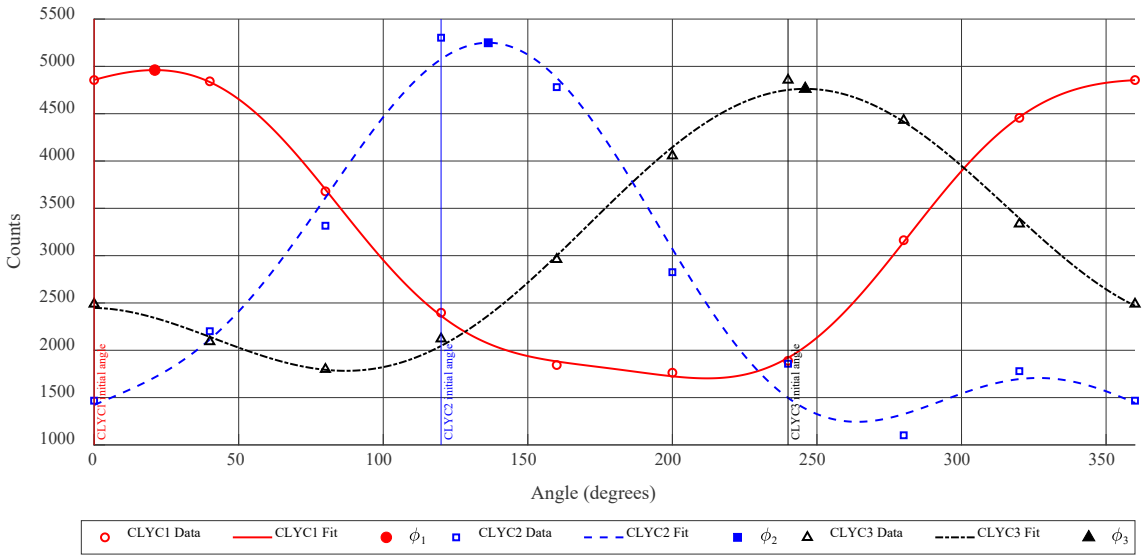
5500
5000
4500
4000
3500
3000
2500
2000
1500
1000
Counts
CLYC1 initial angle
CLYC2 initial angle
CLYC3 initial angle
0
50
100
150
200
250
300
350
Angle (degrees)
CLYC1 Data
CLYC1 Fit
ϕ_1
CLYC2 Data
CLYC2 Fit
ϕ_2
CLYC3 Data
CLYC3 Fit
ϕ_3

(b)

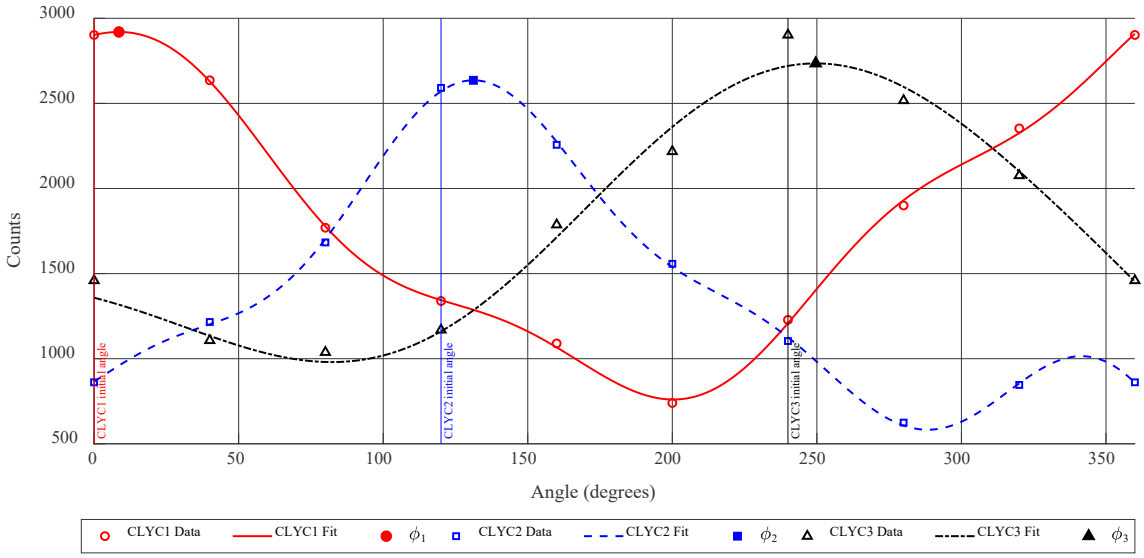

(c)

Figure 7. Two-source directional measurement results for **(a)** ^{137}Cs 662 keV peak; **(b)** ^{60}Co 1.17 MeV peak; **(c)** ^{60}Co 1.33 MeV peak.

Two locations for the ^{239}PuBe source were used in directional measurements. The source was placed at the 0°/360° mark on the detector system turntable in-plane with the detector system ($z = 0$ m) and at 1 m from the center of the system. This setup is shown in Fig. 8. The measurement results for this configuration are shown in Fig. 9a. The MLE evaluation of the source direction was 359° ± 36°; a difference of 1° from the actual source direction.

The source was then moved out to $R = 3$ m from the center of the detector system and remained at a height in-plane with the detector system. The results for this source-detector arrangement are presented in Fig. 9b. The MLE source direction was 19° ± 6°. This deviated from the actual source direction by 19°.

It is hypothesized that the discrepancies observed in source direction can be eliminated by increasing the measurement time at each angle and increasing the angle increments at which measurements are performed (i.e., collect measurements at every 10° instead of 40°). These discrepancies can also be addressed by utilizing a directional detection system of identical CLYC cells of the same size and quality, identical PMTs and identical aluminum housings. In this study, two of the three CLYC detectors used in the three-cell system were the same size. In the directional neutron measurements, the shielded vault caused neutron scattering from concrete walls and the floor. The beam port of the shielded container of the ^{239}PuBe source generated a wide beam of low energy neutrons, thus resulting in the wide angular distribution of neutron emission towards the directional detector. In field measurements at longer distances, this ‘room’ effect will be less important.

Figure 8. Directional measurements using a moderated ^{239}PuBe source.

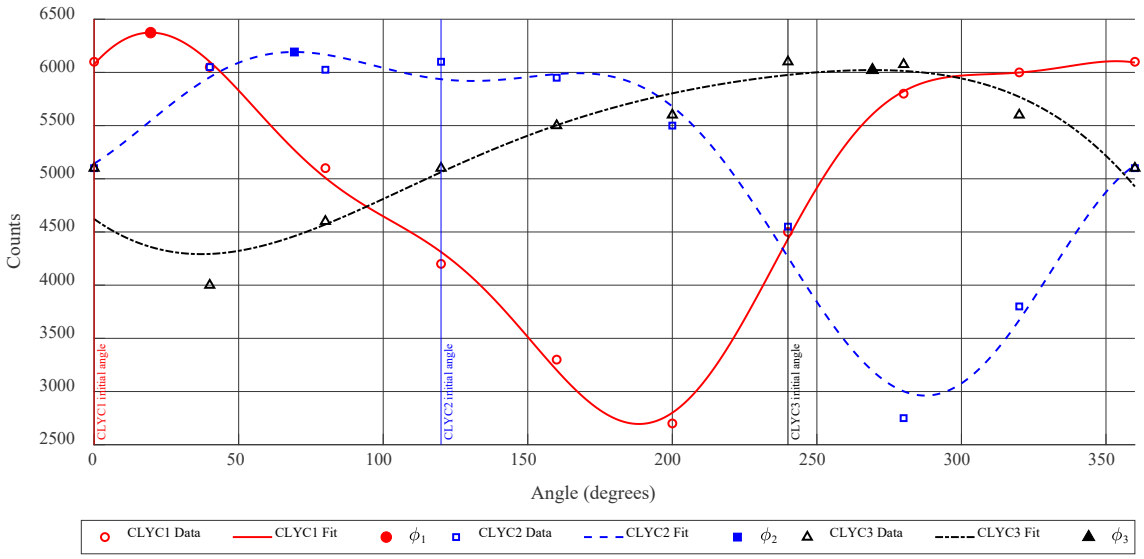

(a)

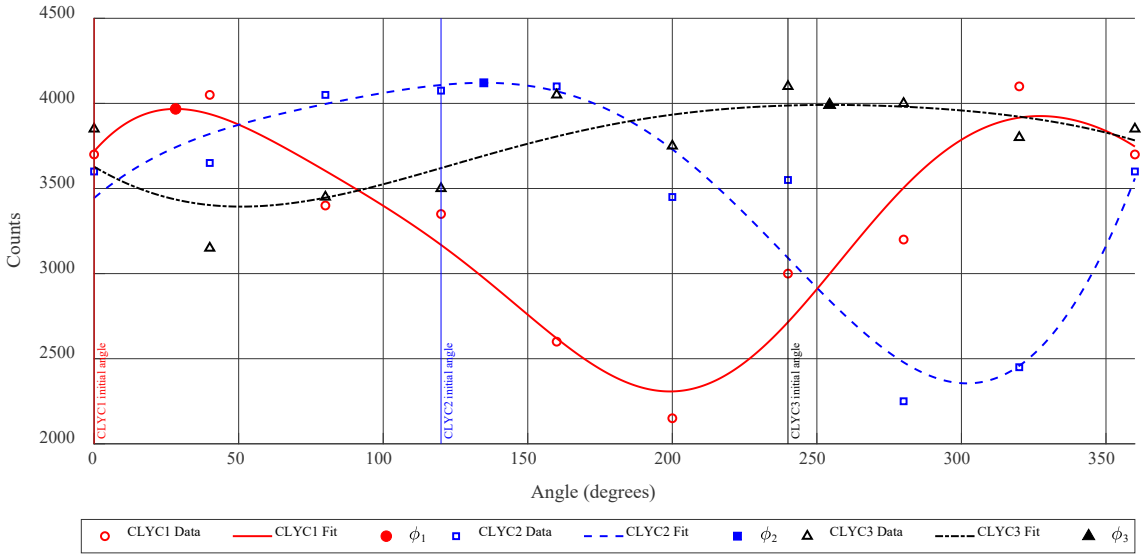

(b)

Figure 9. ^{239}PuBe directional measurement results: **(a)** R = 1 m, z = 0 m; **(b)** R = 3 m, z = 0 m.

Table 1
MLE estimates of angle pointing to the source.

Source Type	Source Location	Actual Source Angle	MLE Source Angle ± σ	Actual vs MLE Angle Difference
^{137}Cs	R = 10 cm, z = 0 cm	0°/360°	5° ± 25°	5°
^{137}Cs	R = 20 cm, z = 0 cm	0°/360°	345° ± 2°	15°
^{137}Cs	R = 10 cm, z = +10 cm	0°/360°	337° ± 16°	23°
^{137}Cs	R = 20 cm, z = +10 cm	0°/360°	6° ± 26°	6°
^{137}Cs + ^{60}Co (^{137}Cs 662 keV used)	R = 10 cm, z = 0 cm	0°/360°	13° ± 8°	13°
^{137}Cs + ^{60}Co (^{60}Co 1.17 MeV used)	R = 10 cm, z = -20 cm	240°	254° ± 6°	14°
^{137}Cs + ^{60}Co (^{60}Co 1.33 MeV used)	R = 10 cm, z = -20 cm	240°	250° ± 1°	10°
^{239}PuBe	R = 1 m, z = 0 m	0°/360°	359° ± 36°	1°
^{239}PuBe	R = 3 m, z = 0 m	0°/360°	19° ± 6°	19°

4. Conclusion

A detector system consisting of an array of CLYC-based detectors was studied for directional, simultaneous thermal neutron and gamma-ray measurements. The detector system was tested using a single ^{137}Cs photon source, two gamma sources simultaneously (^{137}Cs and ^{60}Co), and a moderated ^{239}PuBe source in various configurations. Directional measurements were carried out through 360° rotation in increments of 40°. The MLE algorithm was used to estimate the most probable direction to the source based on counts measured in each of the three elpasolite cells. The evaluation of the cell's responses showed that the three-cell array is feasible to determine the direction to a point-like gamma-ray source and thermal neutron source simultaneously.

For most configurations, the direction to a source was estimated within the standard deviation. The maximum difference between the actual versus MLE angle of the discrepant results was 23°. This difference can be reduced by increasing time of measurement and increasing the number of increments to be measured in 360°. The difference

can also be reduced by homogenizing the detector system (i.e., same size/quality CLYC cells, same PMTs, same housings) and using larger scintillator cells to maximize detection efficiency. The directional measurements using the system for search of point neutron sources at longer distances in the field will demonstrate better agreement between the actual and MLE angles.

This three-CLYC detector system with the MLE enabled source localization would allow an end-user to search for missing/stolen radiological or nuclear materials, WMDs and RDDs, with improved direction estimates at each step while approaching the source. This system could also be used in a variety of other applications including environmental safety and waste management.

Acknowledgments

This manuscript has been authored by Mission Support and Test Services, LLC, under Contract No. DE-NA0003624 with the U.S. Department of Energy and supported by the Site-Directed Research and Development Program, NA USDOE National Nuclear Security Administration (NNSA). The United States Government retains and the publisher, by accepting the article for publication, acknowledges that the United States Government retains a non-exclusive, paid-up, irrevocable, worldwide license to publish or reproduce the published form of this manuscript, or allow others to do so, for United States Government purposes. The U.S. Department of Energy will provide public access to these results of federally sponsored research in accordance with the DOE Public Access Plan (http://energy.gov/downloads/doe-public-access-plan). The views expressed in the article do not necessarily represent the views of the U.S. Department of Energy or the United States Government. DOE/NV/03624--0961..

The authors acknowledge the professional staff of RMD, Watertown, Massachusetts, for the production of the scintillators, for providing these detectors to the Remote Sensing Laboratory, and for their support and advice.

References

[1] J. Doyle, Nuclear Safeguards, Security and Nonproliferation, Elsevier, Oxford, UK, 2008.

[2] R. Runkle, Neutron sensors and their role in nuclear nonproliferation, Nuclear Instruments and Methods in Physics Research A, 652 (2011) 37-40.

[3] D.M. Trombetta, M. Klintefjord, K. Axell, B. Cederwall, Fast neutron- and γ-ray coincidence detection for nuclear security and safeguards applications. Nuclear Instruments and Methods in Physics Research A, 927 (2019) 119-124.

[4] J. Hite, J. Mattingly, D. Archer, M. Willis, A. Rowe, K. Bray, J. Carter, J. Ghawaly, Localization of a radioactive source in an urban environment using Bayesian Metropolis methods. Nuclear Instruments and Methods in Physics Research A, 915 (2019) 82-93.

[5] K. Moody, P. Grant, I. Hutcheon, Y. Varoufakis, Nuclear Forensic Analysis, Taylor & Francis, New York, NY, 2014.

[6] International Atomic Energy Agency (IAEA), Sealed Radioactive Sources, Oct 2013, available at https://www.iaea.org/sites/default/files/sealedradsources1013.pdf (accessed on June 29, 2020).

[7] G. Steinhauser, A. Brandl, T. Johnson, Comparison of the Chernobyl and Fukushima nuclear accidents: a review of the environmental impacts. Science of the Total Environment, 471 (2014) 800-817.

[8] Y. Sanada, T. Torii, Aerial radiation monitoring around the Fukushima Daiichi Nuclear Power Plant using an unmanned helicopter. Journal of Environmental Radioactivity, 139 (2015) 294-299.

[9] W. Barletta, The Fukushima Dai-ichi accident and its implications for the safety of nuclear power. Nuclear Instruments and Methods in Physics Research A, 817 (2016) A1-A3.

[10] T. Kurihara, K. Tanada, J. Kataoka, H. Hosokoshi, S. Mochizuki, L. Tagawa, H. Okochi, Y. Gotoh, Precision spectroscopy of cesium-137 from the ground to 150 m above in Fukushima. Nuclear Instruments and Methods in Physics Research A, 978 (2020) 164414.

[11] N.E. Stauff, T.K. Kim, T.A. Taiwo, Variations in nuclear waste management performance of various fuel-cycle options. Journal of Nuclear Science and Technology, 52 (2015) 1058-1073.

[12] M. Greenberg, K. Lowrie, J. Burger, C. Powers, M. Gochfeld, H. Mayer, Preferences for alternative risk management policies at the United States major nuclear weapons legacy sites. Journal of Environmental Planning and Management, 50(2) (2007) 187-209.

[13] D.L. Chichester, J.D. Simpson, M. Lemchak, Advanced compact accelerator neutron generator technology for active neutron interrogation field work. Journal of Radioanalytical and Nuclear Chemistry, 271 (2007) 629-637.

[14] A. Barzilov, P. Womble, Study of Doppler broadening of gamma-ray spectra in 14-MeV neutron activation analysis. Journal of Radioanalytical and Nuclear Chemistry, 301 (2014) 811-819.

[15] J. Bendahan, Review of active interrogation techniques. Nuclear Instruments and Methods in Physics Research A, 954 (2020) 161120.

[16] A. Poitrasson-Rivière, J.K. Polack, M.C. Hamel, D.D. Klemm, K. Ito, A.T. McSpaden, M. Flaska, S.D. Clarke, S.A. Pozzi, A. Tomanin, P. Peerani, Angular-resolution and material-characterization measurements for a dual-particle imaging system with mixed-oxide fuel. Nuclear Instruments and Methods in Physics Research A, 797 (2015) 278-284.

[17] J. Hartman, A. Pour Yazdanpanah, A. Barzilov, E. Regentova, 3D imaging using combined neutron-photon fan-beam tomography: A Monte Carlo study. Applied Radiation and Isotopes, 111 (2016) 110-116.

[18] G.F. Knoll, Radiation Detection and Measurement, 4th ed., Wiley, New York, 2010.

[19] N. Zaitseva, B. Rupert, I. Pawelczak, A. Glenn, H.P. Martinez, L. Carman, M. Faust, N. Cherepy, S. Payne, Plastic scintillators with efficient neutron/gamma pulse shape discrimination. Nuclear Instruments and Methods in Physics Research A, 668 (2012) 88-93.

[20] D. Cester, G. Nebbia, L. Stevanato, F. Pino, G. Viesti, Experimental tests of the new plastic scintillator with pulse shape discrimination capabilities EJ-299-33. Nuclear Instruments and Methods in Physics Research A, 735 (2014) 202-206.

[21] J. Qin, C. Lai, B. Ye, R. Liu, X. Zhang, L. Jiang, Characterizations of BC501A and BC537 liquid scintillator detectors. Applied Radiation and Isotopes, 104 (2015) 15-24.

[22] K. Biswas, M.H. Du, Energy transport and scintillation of cerium-doped elpasolite Cs_2LiYCl_6: hybrid density functional calculations. Physical Review B, 86 (2012) 014102.

[23] J. Glodo, R. Hawrami, K.S. Shah, Development of Cs_2LiYCl_6 scintillator. Journal of Crystal Growth, 379 (2013) 73-78.

[24] R. Machrafi, N. Khan, A. Miller, Response functions of Cs_2LiYCl_6:Ce scintillator to neutron and gamma radiation. Radiation Measurements 70 (2014) 5-10.

[25] N. D'Olympia, P. Chowdhury, C.J. Guess, T. Harrington, E.G. Jackson, S. Lakshmi, C.J. Lister, J. Glodo, R. Hawrami, K.S. Shah, U. Shirwadkar, Optimizing Cs_2LiYCl_6 for fast neutron spectroscopy. Nuclear Instruments and Methods in Physics Research A, 694 (2012) 140-146.

[26] M.B. Smith, T. Achtzehn, H.R. Andres, E.T.H. Clifford, P. Forget, J. Glodo, R. Hawrami, H. Ing, P. O'Doughtery, K.S. Shah, U. Shirwadkar, L. Soundara-Pandian, J. Tower, Fast neutron measurements using Cs_2LiYCl_6:Ce (CLYC) scintillator, Nuclear Instruments and Methods in Physics Research A, 784 (2015) 162-167.

[27] E.V.D. Van Loef, P. Dorenbos, C.W.E. Van Eijk, K.W. Krämer, H.U. Güdel, Scintillation and spectroscopy of the pure and Ce^{3+}-doped elpasolites: Cs_2LiYX_6 (X = Cl; Br). Journal of Physics: Condensed Matter, 14 (2002) 8481-8496.

[28] J. Glodo, E. Van Loef, R. Hawrami, W.M. Higgins, A. Churilov, U. Shirwadkar, K.S. Shah, Selected properties of Cs_2LiYCl_6, $Cs_2LiLaCl_6$, and $Cs_2LiLaBr_6$ scintillators. IEEE Transactions on Nuclear Science, 58 (2011) 333-338.

[29] P. Rodnyi, Core-valence luminescence in scintillators. Radiation Measurements, 38 (2004) 343-352.

[30] N. D'Olympia, P. Chowdhury, C.J. Lister, J. Glodo, R. Hawrami, K. Shah, U. Shirwadkar, Pulse-shape analysis of CLYC for thermal neutrons, fast neutrons, and gamma-rays. Nuclear Instruments and Methods in Physics Research A, 714 (2013) 121-127.

[31] A. Giaz, L. Pellegri, F. Camera, N, Blasi, S. Brambilla, S. Ceruti, B. Million, S. Riboldi, C. Cazzaniga, G. Gorini, M. Nocente, A. Pietropaolo, M. Pillon, M. Rebai, M. Tardocchi, The CLYC-6 and CLYC-7 response to gamma-rays, fast and thermal neutrons. Nuclear Instruments and Methods in Physics Research A, 810 (2016) 132-139.

[32] Radiation Monitoring Devices, Gamma-Neutron Scintillator Properties - CLYC, available at https://www.dynasil.com//assets/CLYC-Gamma-Neutron-Scintillator-Properties.pdf (accessed on June 29, 2020).

[33] C.M. Bartle, G.V.M. Williams, An efficient directional fast neutron sensor for a mixed radiation field. Rad. Meas., 46 (2011) 1716-1719.

[34] A. Weltz, B. Torres, L. McElwain, R. Dahal, J. Huang, I. Bhat, J. Lu, Y. Danon, Development of a modular directional and spectral neutron detection system using solid-state detectors. Nuclear Instruments and Methods in Physics Research A, 792 (2015) 28-37.

[35] Y. Fu, Y. Tian, Y. Li, J. Yang, J. Li, Directional fast neutron detection using a time projection chamber and plastic scintillation detectors. Nuclear Instruments and Methods in Physics Research A, 954 (2020) 161445.

[36] Y. Sato, K. Minemoto, M. Nemoto, T. Torii, Construction of virtual reality system for radiation working environment reproduced by gamma-ray imagers combined with SLAM technologies. Nuclear Instruments and Methods in Physics Research A, 976 (2020) 164286.

[37] D. Goodman, J. Xia, Z. He, Qualitative measurement of spatial shielding isotopics via Compton imaging neutron-induced gamma rays using 3-D CdZnTe detectors. Nuclear Instruments and Methods in Physics Research A, 935 (2019) 214-221.

[38] P. Guss, S. Mukhopadhyay, Dual gamma neutron directional elpasolite detector, in: SPIE Proc. 8854 (2013) 885402.

[39] P. Guss, T. Stampahar, S. Mukhopadhyay, J. Lee, K. Shah, M. Squillante, W. Higgins, Novel deployment of elpasolites as a dual gamma-neutron directional detector, in: Site Directed Research & Development, Remote Sensing Laboratory-Nellis, 2013.

[40] A. Guckes, A. Barzilov, P. Guss, Directional detection of neutrons and photons using elpasolites: computational study, Radiations Measurements, 124 (2019) 127 - 131.

[41] S.R. Eliason, Maximum likelihood estimation, Sage Publications, Newbury Park, CA, 1993.

[42] A. Lintereur, J. Ely, J. Stave, B. Macdonald, Neutron and gamma ray pulse shape discrimination with polyvinyltoluene, PNNL-21609, Pacific Northwest National Laboratory, Mar 2012, available at https://www.pnnl.gov/main/publications/external/technical_reports/PNNL-21609.pdf (accessed on June 29, 2020).